UNIVERSITÉ PARIS 7 – DENIS DIDEROT
INSTITUT DE PHYSIQUE DE L'UNIVERSITÉ DE LETTONIE

Instabilités hydrodynamiques des liquides magnétiques miscibles et non miscibles dans une cellule de Hele-Shaw

Samaisošos un nesamaisošos magnētisko šķidrumu hidrodinamiskās nestabilitātes Hele-Šou šūnā

Max IGONIN

Directeurs de thèse: Jean-Claude BACRI
Andrejs CĒBERS

Outline

I. Presentation of the problem and the motivating experiments. The governing equations.

II. Linear stability analysis for a miscible ferrofluid in a Hele-Shaw cell.

III. Immiscible interfaces: The nonlinear simulations of the Saffman–Taylor instability by the boundary-integral method.

Ferrofluids and convection

- Ferrofluid is a colloidal suspension of magnetic particles.
  - Particles are nanosized and monodomain. The dipolar colloid is stable against aggregation and sedimentation. “Miscible” ferrofluids.
  - In a dilute ferrofluid, the particles interact through the self-magnetic (demagnetizing) field of the ensemble.

- Ferrofluid is a “superparamagnetic” media.
  - In a uniform applied field, if the ferrofluid is inhomogeneous or is appropriately arranged in space, its self-magnetic field is inhomogeneous as well.
  - In an inhomogeneous resulting field, a force is exerted on particles.
  - Particles generally entrain the carrier owing to the Stokes drag. Then the magnetophoresis can be neglected.

Ferrofluids and convection

- A ferrofluid parcel is driven into a stronger resulting field – i.e. *away* from the main volume of the ferrofluid.
  - a convective instability can develop even though
  - surface tension or viscosity and diffusion tend to stabilize the perturbations. The relative importance of the destabilizing effect against the regularizing ones is given by the magnetic Bond number Bm and by a Rayleigh number Cm, respectively.
  - Unlike other instabilities, the direction of the driving force $\vec{f}_m = M\vec{\nabla}H$ is generally variable in both space and time.

Experimental background: Diffusion fronts

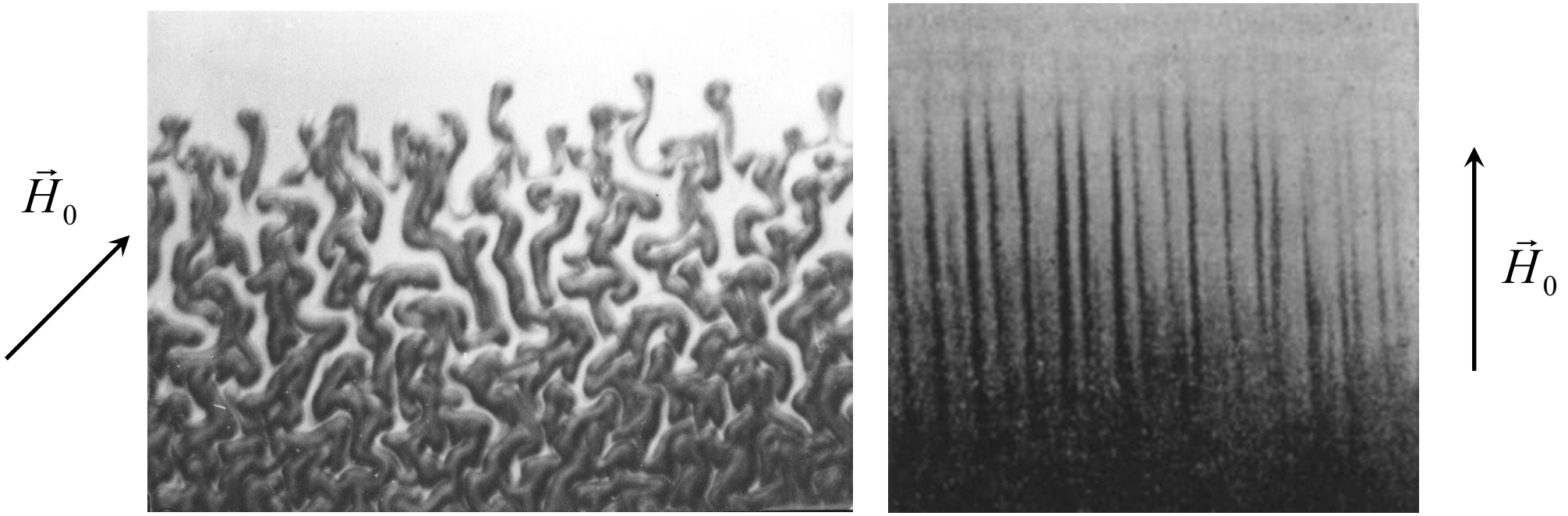

Labyrinthine (*left*) and peak (*right*) instabilities at the diffusion fronts between a ferrofluid and its pure carrier liquid (Maiorov & Cebers, 1983). The length scale of convection pattern: $\sim h = 100$ μm.

Maiorov & Cebers, Magnetohydrodynamics (N.Y.) 19, 376 (1983).

Experimental background: Transient optical gratings in magnetized ferrofluids

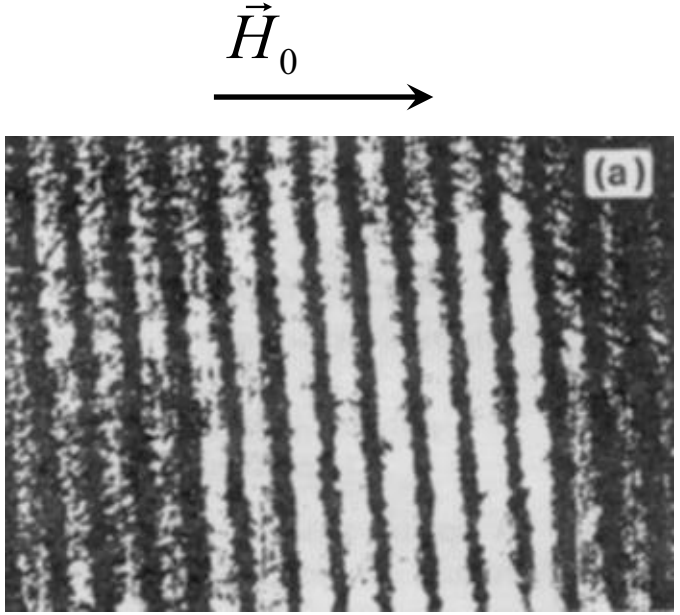

Effective diffusion coefficient increases in the peak field (Bacri et al., 1995)

- The magnetophoresis in the inhomogeneous demagnetizing field
- A micro-scale convection?

(Mezulis & Blums, 2004)

Bacri et al., PRL 74, 5032 (1995).

Experimental background: other related experiments

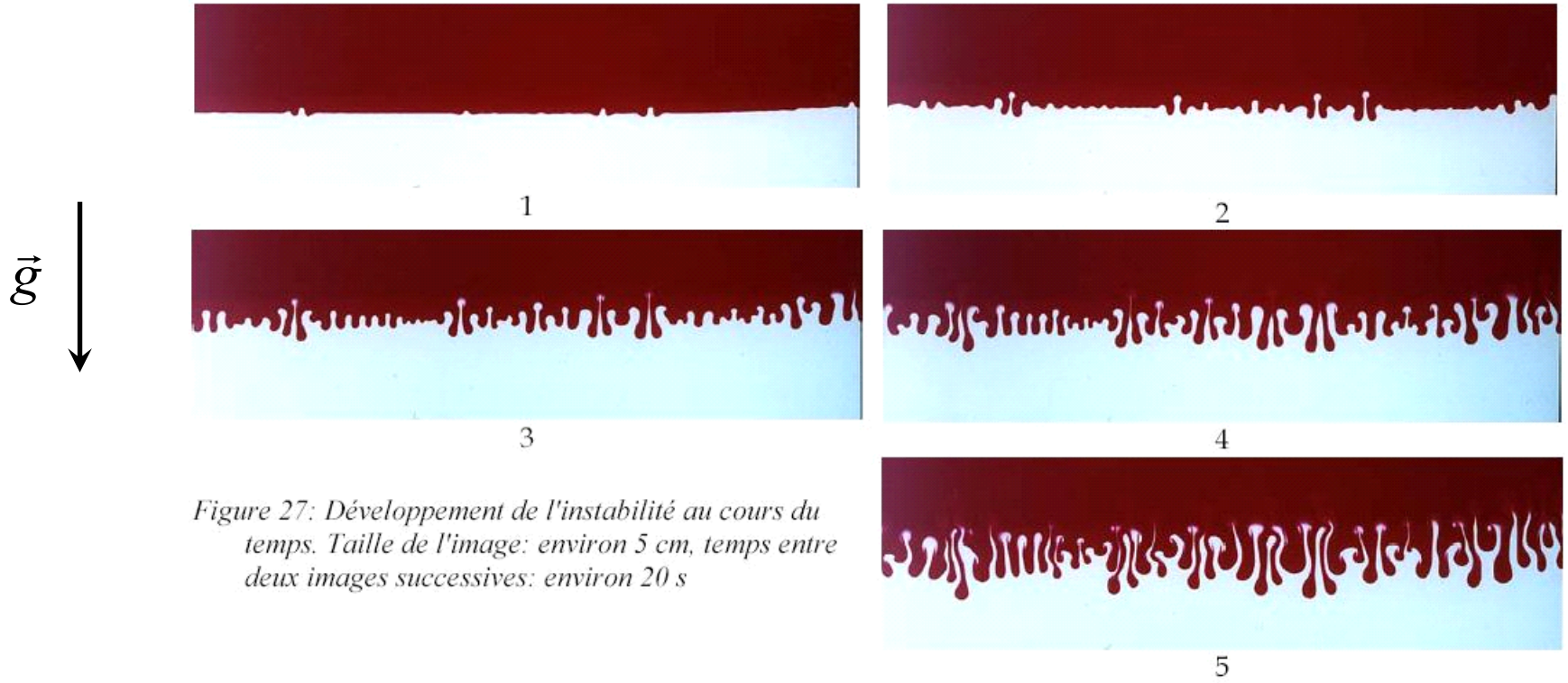

Figure 27: Développement de l'instabilité au cours du temps. Taille de l'image: environ 5 cm, temps entre deux images successives: environ 20 s

Fernandez, Kurowski, Petitjeans, and Meiburg.
J. Fluid Mech. 451, 239 (2002).
www.pmmh.espci.fr (Galerie de photographies)

Lajeunesse et al., PRL 79, 5254 (1997). $\Longrightarrow$

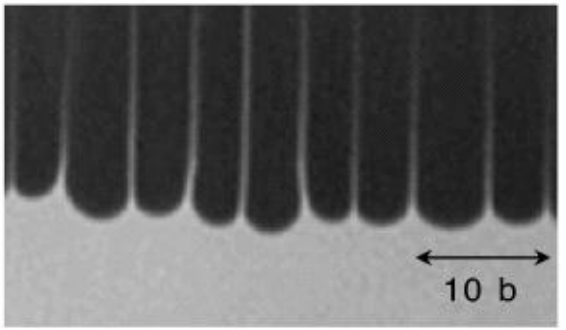

b is h = 1 mm or 1.92 mm

Saffman-Taylor and Rayleigh-Taylor instabilities with immiscible ferrofluids

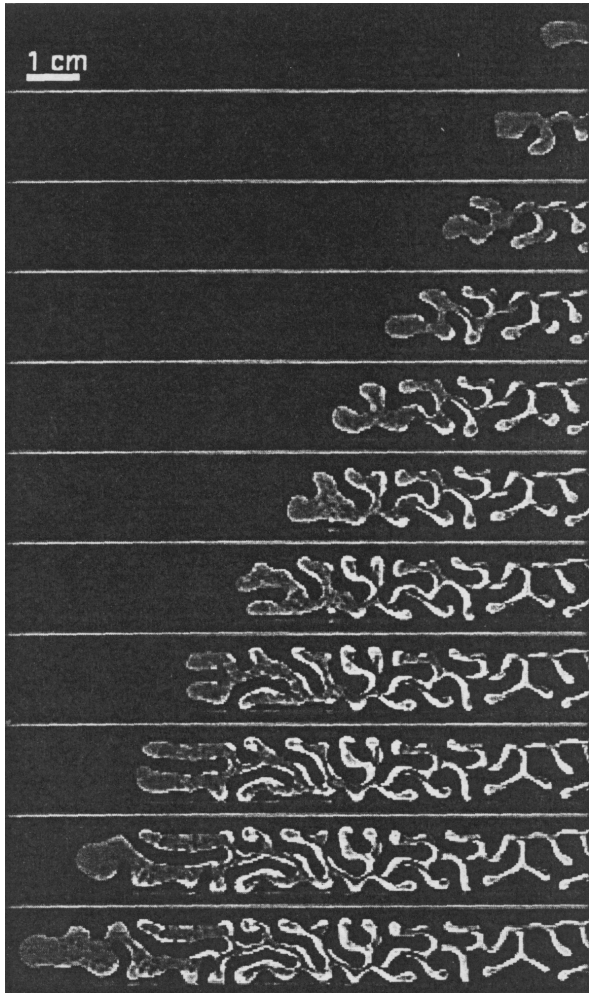

$\vec{H}_0$

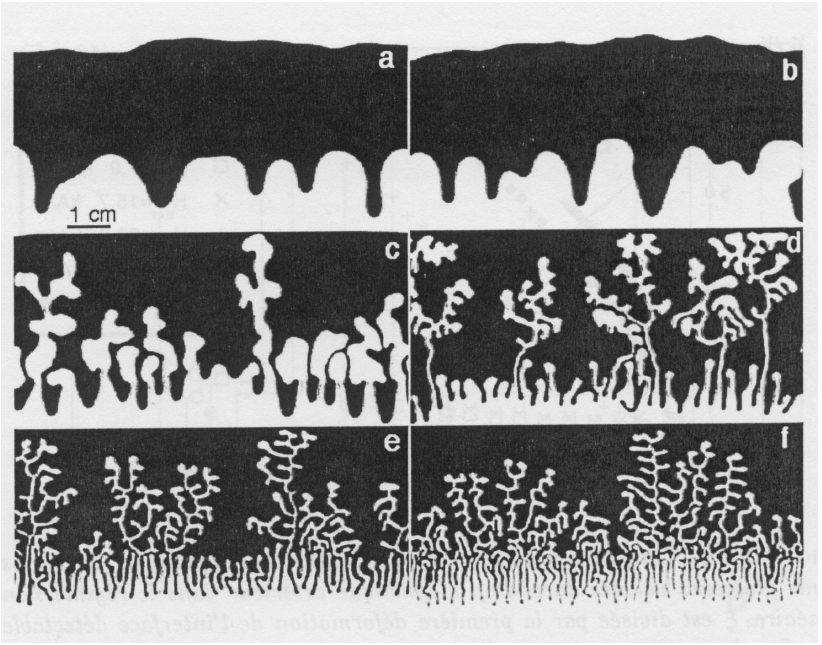

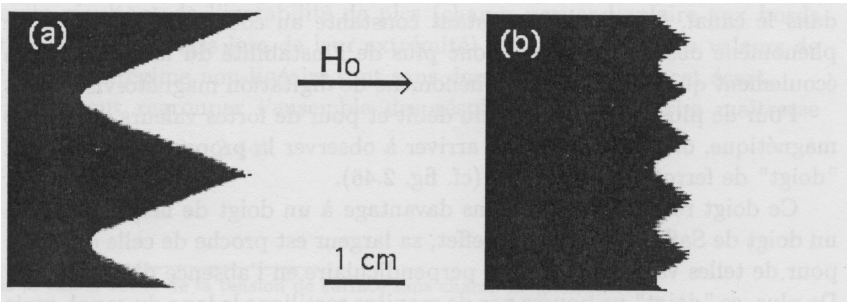

G. Pacitto, UP7 thesis; Pacitto et al., PRE 62, 7941 (2000); Pacitto, Flament, and Bacri, Phys. Fluids 13, 3196 (2001).

Questions and problems

- The linear stability for inhomogeneous ferrofluids is almost unexplored.
- The convection occurs on a microscale. What selects a finite length scale at the interface?
- Instability can importantly increase the length of the “interface,” thus facilitating the laminar mixing. Can be important in *microfluidics*.
- Relation to the well-studied immiscible problem.

The governing equations: diffusion, Korteweg stresses, and gap-averaging

- a convection–diffusion equation $\dfrac{\partial c}{\partial t} + (\vec{u} \cdot \vec{\nabla})c = D\Delta c$

  Passive scalar in a Hele-Shaw cell: $D_{\text{eff}} / D - 1 = \dfrac{1}{210}\text{Pe}^2$

  (the Taylor dispersion; $\text{Pe} = < u > h / D$)

- Active scalar, $\eta = \eta(c)$.

  Non-Poiseuille velocity profiles.

  The isolines of concentration across the cell:

  shocks and central protrusions. The relation to a 3D instability.

  Petitjeans & Maxworthy, J. Fluid Mech. 326, 37 (1996);
  Chen & Meiburg, 57; Lajeunesse et al., J. Fluid Mech. 398, 299 (1999).

- "Very active" scalar: concentration or density gradients generate mechanical Korteweg stresses. Under discussion.

  Joseph, Eur. J. Mech. B / Fluids 9, 565 (1990)

→

The governing equations: the equation of motion

- At a constant viscosity η
  the 3D Stokes equation is exact:

$$-\vec{\nabla}p+\eta\Delta\vec{u}+\vec{f}_m=0$$

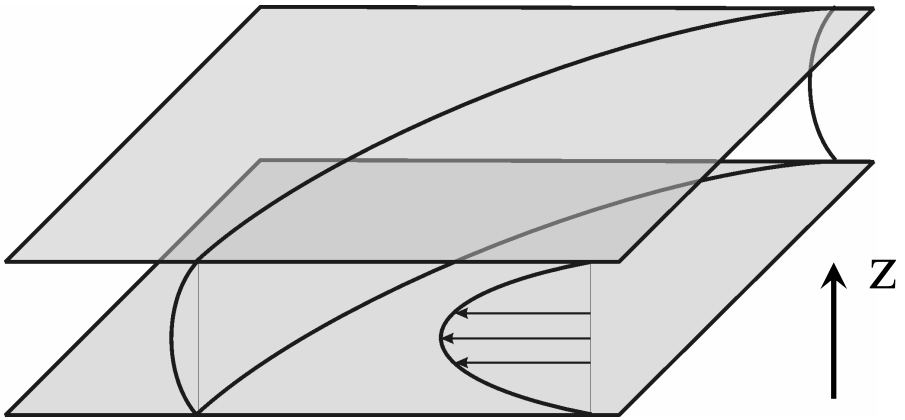

- 2D Brinkman

$$\boxed{-\vec{\nabla}<p>+(\eta\Delta_\perp-\alpha)<\vec{u}>+<\vec{f}_m>=0} \qquad \eta<\partial^2\vec{u}/\partial z^2>=-\alpha<\vec{u}>$$

  - for a weakly perturbed straight interface
  - Prefactors for α,η are usually not known

Zeng, Yortsos, and Salin, Phys. Fluids 15, 3829 (2003).

- 2D Darcy: the usual approximation (the Poiseuille profile)

$$-\vec{\nabla}<p>-\alpha<\vec{u}>+<\vec{f}_m>=0 \qquad \alpha=12\eta/h^2$$

Governing equations: the magnetostatic force

Magnetostatics: $\mathrm{rot}\,\vec{H} = 0,\ \mathrm{div}\,\vec{B} = 0$. Ponderomotive force: $\vec{f}_m = M\vec{\nabla}H.$

$M << H$: $M = m_0 c$, where $m_0 = \mathrm{const}$ is the average moment along $\vec{H}$.

The gap-averaging at $\varphi \to 0$ gives the force ($\mathrm{rot} < \vec{f}_m > \neq 0$ generally):

$$< \vec{f}_m >= -\frac{2m_0 c}{h}\vec{\nabla}\Psi \qquad \text{(labyrinthine field)}$$

$$< \vec{f}_m >= m_0 c\vec{\nabla}\,\partial\Psi/\partial x \qquad \text{(peak field along the } x\text{-axis)}$$

Averaged magnetostatic potential Ψ :

$$\Psi(\vec{r},t) = m_0 \int c(\vec{r}',t)K(\vec{r}'-\vec{r})\,\mathrm{d}S' \qquad \text{with} \quad K(\vec{\rho}) = 1/\rho - 1/\sqrt{\rho^2+h^2}$$

$$\frac{\partial\Psi}{\partial x} = \frac{2m_0}{h}\int_{-\infty}^{+\infty}\int_{-\infty}^{+\infty}(x-x')\frac{\partial c}{\partial x'}J\left(\sqrt{(x-x')^2+(y-y')^2}\right)\mathrm{d}x'\,\mathrm{d}y'$$

$$\text{with} \quad J(\rho) = \left(\sqrt{\rho^2+h^2}-\rho\right)/\rho^2$$

Part II.

Linear stability analysis for a miscible ferrofluid in a Hele-Shaw cell.

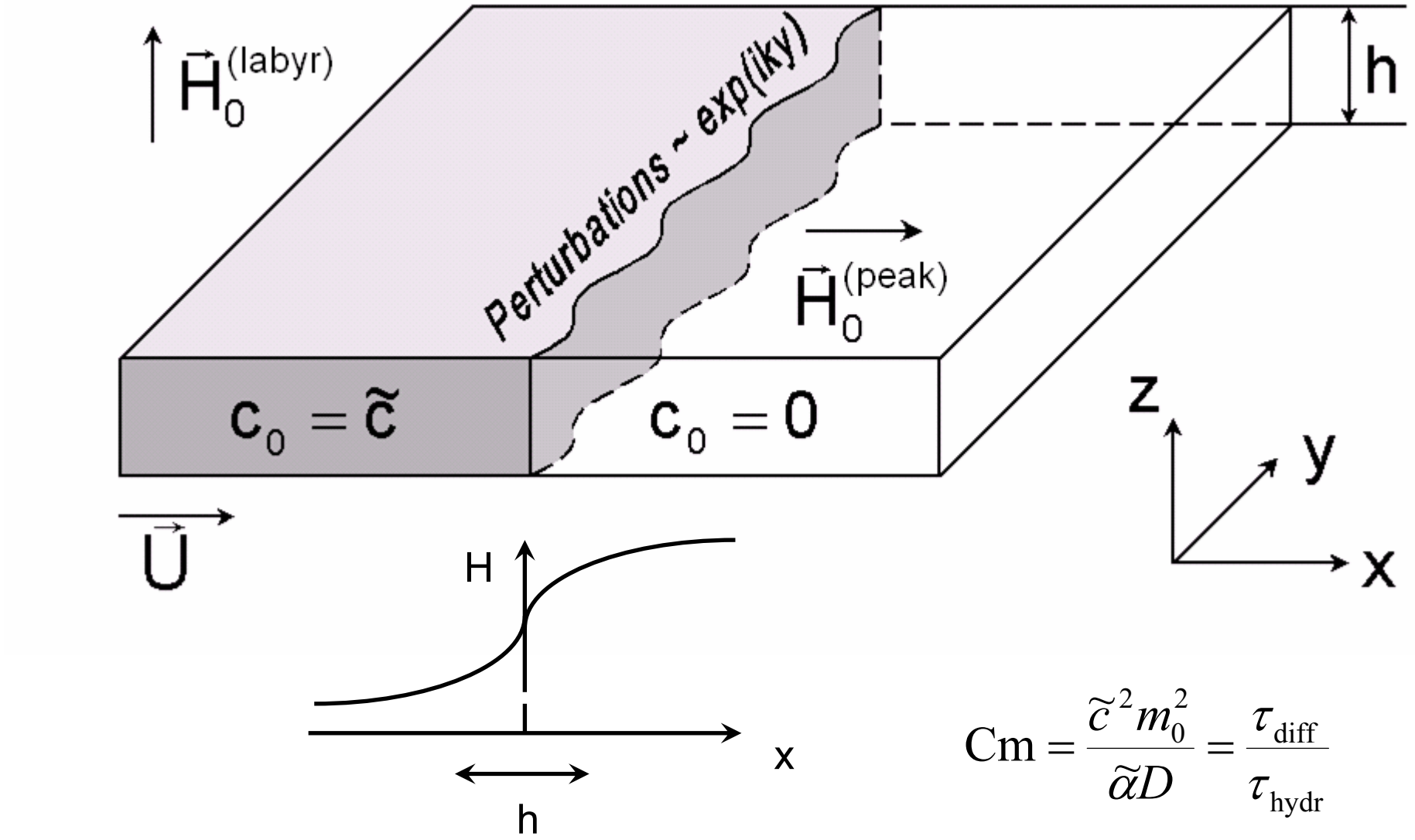

$$\mathrm{Cm} = \frac{\tilde{c}^2 m_0^2}{\tilde{\alpha} D} = \frac{\tau_{\mathrm{diff}}}{\tau_{\mathrm{hydr}}}$$

Perturbations $\exp(iky + \lambda t)$; QSSA

Analytically: the step-like concentration distribution

Numerically: smooth concentration distributions $c_1 = 0.5\,\mathrm{erfc}\left(0.5x/\sqrt{t_0}\right)$

in units $\tilde{c}, h, h^2/D$.

Analytical dispersion relations for the step-like concentration (Darcy's law)

The neutral curve for the peak instability

$$\frac{1}{\mathrm{Cm}} = \frac{\pi}{2} + \frac{2}{3k} - \frac{2-k^2}{3} K_1(k) - \frac{k}{3} K_0(k) + \left(1 - \frac{k^2}{3}\right) \mathrm{Ki}_1(k) - \mathrm{f}(2k)$$

$$\mathrm{Ki}_1(k) = \int_k^{+\infty} K_0(t)\,\mathrm{d}t \qquad \mathrm{f}(a) = \frac{2}{a}\left(\gamma + \ln a - \mathrm{ci}\, a \cos a - \mathrm{si}\, a \sin a\right)$$

$$\gamma = 0.5772..$$

The dispersion relation for the labyrinthine instability

$$\mathrm{Cm}\left[2J(s,k) - k\,\mathrm{f}\left(k(s+1)\right)\right] + \frac{a_1 + a_2}{2} ks + \frac{b_1 + b_2}{4} \frac{\mathrm{Pe}}{s+1} = 0 \qquad s = \sqrt{1 + \lambda / k^2}$$

$$J(s,q) = \int_0^{+\infty} \exp(-sz)\left[K_0(z) - K_0\left(\sqrt{z^2 + q^2}\right)\right] \mathrm{d}z$$

Labyrinthine instability at the sharp interface: the dispersion curves

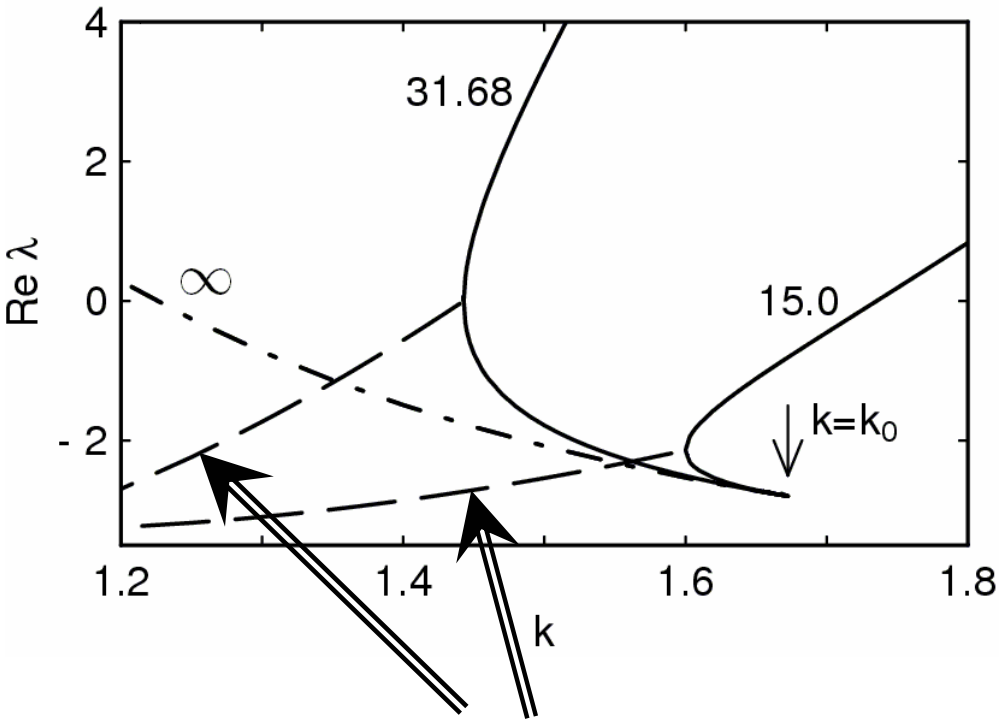

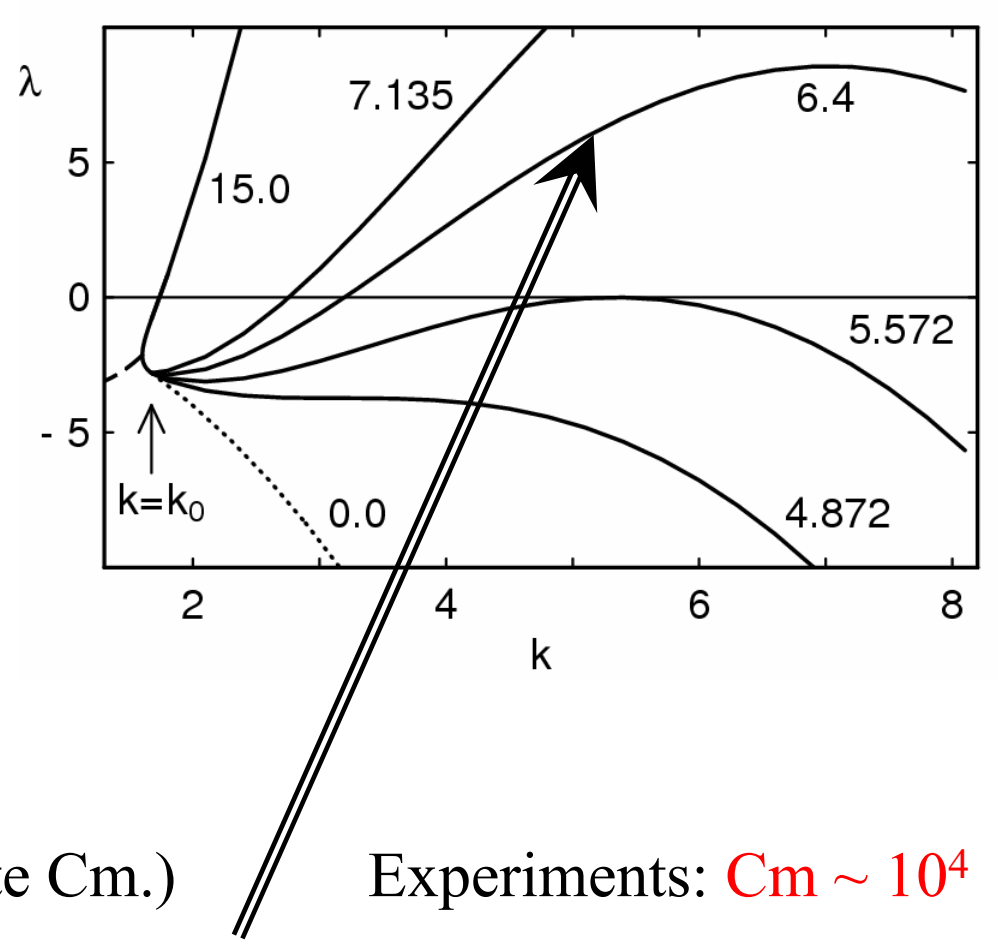

Oscillations

(Numbers near the curves indicate Cm.)

Experiments: Cm ~ 10^4

Asymptotically $\lambda = -k^2 + 2\,\mathrm{Cm}\,k\left(\ln(k/2) + K_0(k) + \gamma\right)$

The number of instability modes: Application of the Cauchy principle of argument

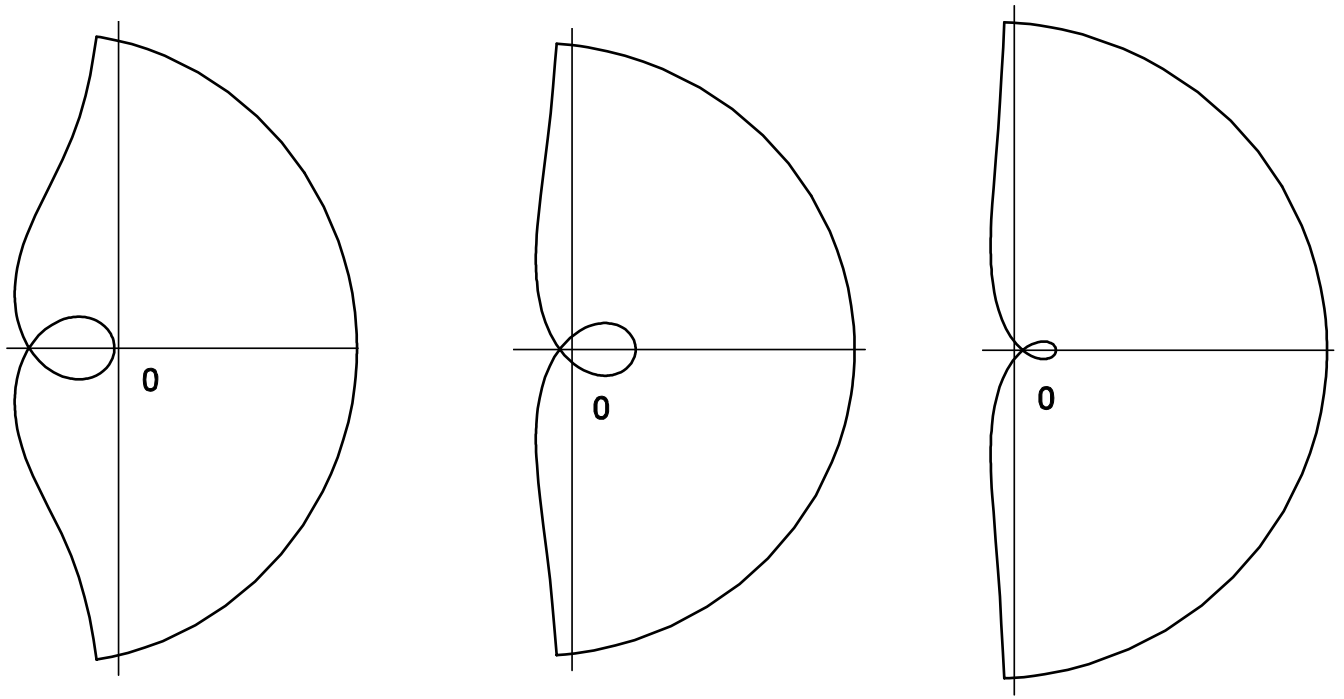

1 turn 2 turns 0 turns

Image of a semi-circle under a complex transform defined by the dispersion relation. The number of discrete modes equals the number of turns the point makes around the origin as it follows the image curve.

The numerical stability analysis

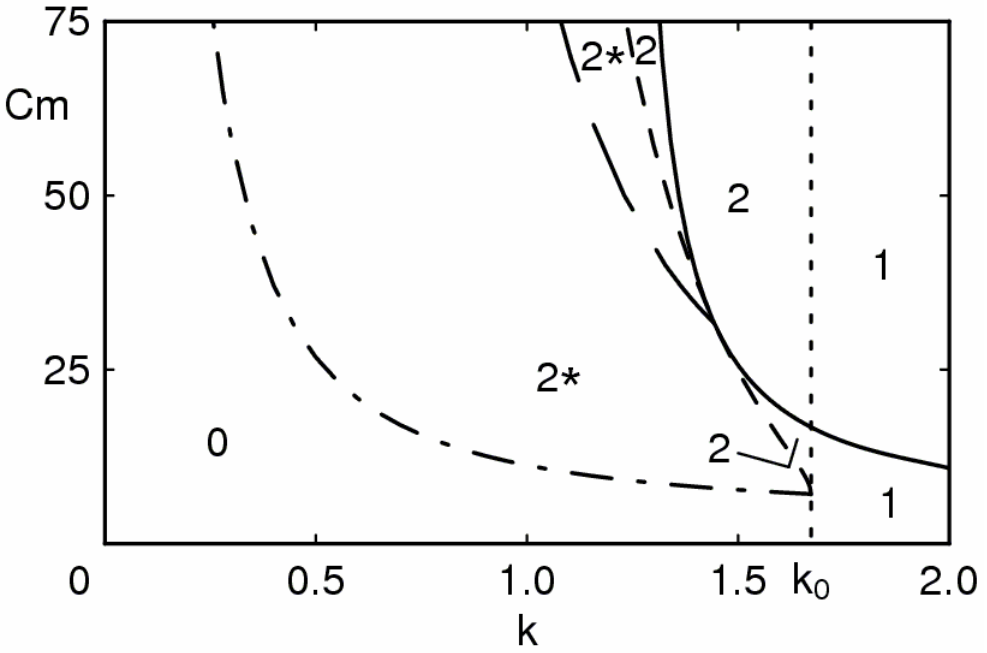

Cm	Wavenumber k								
	0.14	0.2	0.3	0.5	0.7	1.0	1.4	2.0	3.0
300	2*	2*	2* / 2	3	3 / 2	3 / 2	3 / 2	3 / 2	3 / 2
150	2*	2*	2*	2	3 / 2	2	2	3 / 2	3 / 2
100	2*	2*	2*	2* / 2	3 / 1	2	2	2	3 / 2
75	2*	2*	2*	2* / 2	2 / 1	2 / 1	2	2	2
50	0	2*	2*	2* / 2	2 / 1	1	2 / 1	2	2
30	0	0	2*	2* / 2	2 / 1	1	1	2 / 1	2 / 1
20	0	0	0	2*	2* / 1	1	1	1	2 / 1
10	0	0	0	0	2* / 1	1	1	1	1
5	0	0	0	0	0 / 1	1	1	1	1
3	0	0	0	0	0 / 1	1	1	1	1

The analytical stability diagram (the number and type of modes and neutral curves) for the sharp interface ($t_0 = 0$). The asymptotic formulas for most curves are available; e.g. for the oscillatory neutral curve we have $16/\mathrm{Cm} = k^5(-\ln k)$

The number and type of numerical modes at $t_0 = 0.01$ satisfying the condition for the discrete spectrum $\mathrm{Re}\, s > 0$. The Brinkman results, if they differ, follow a slash.

A "*" denotes an oscillatory (complex-conjugated) pair of modes.

The numerical growth increment

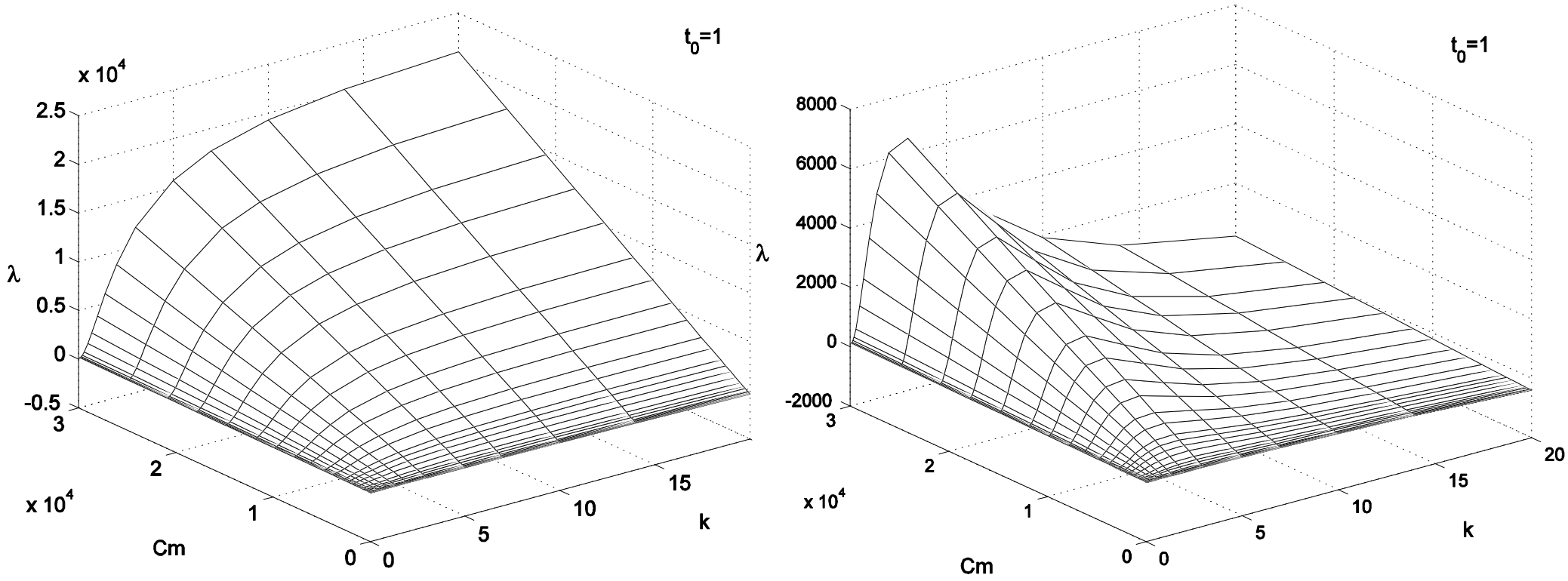

The Darcy (*left*) and Brinkman (*right*) dominant modes (labyrinthine instability, $t_0 = 1$).

The most unstable wave number

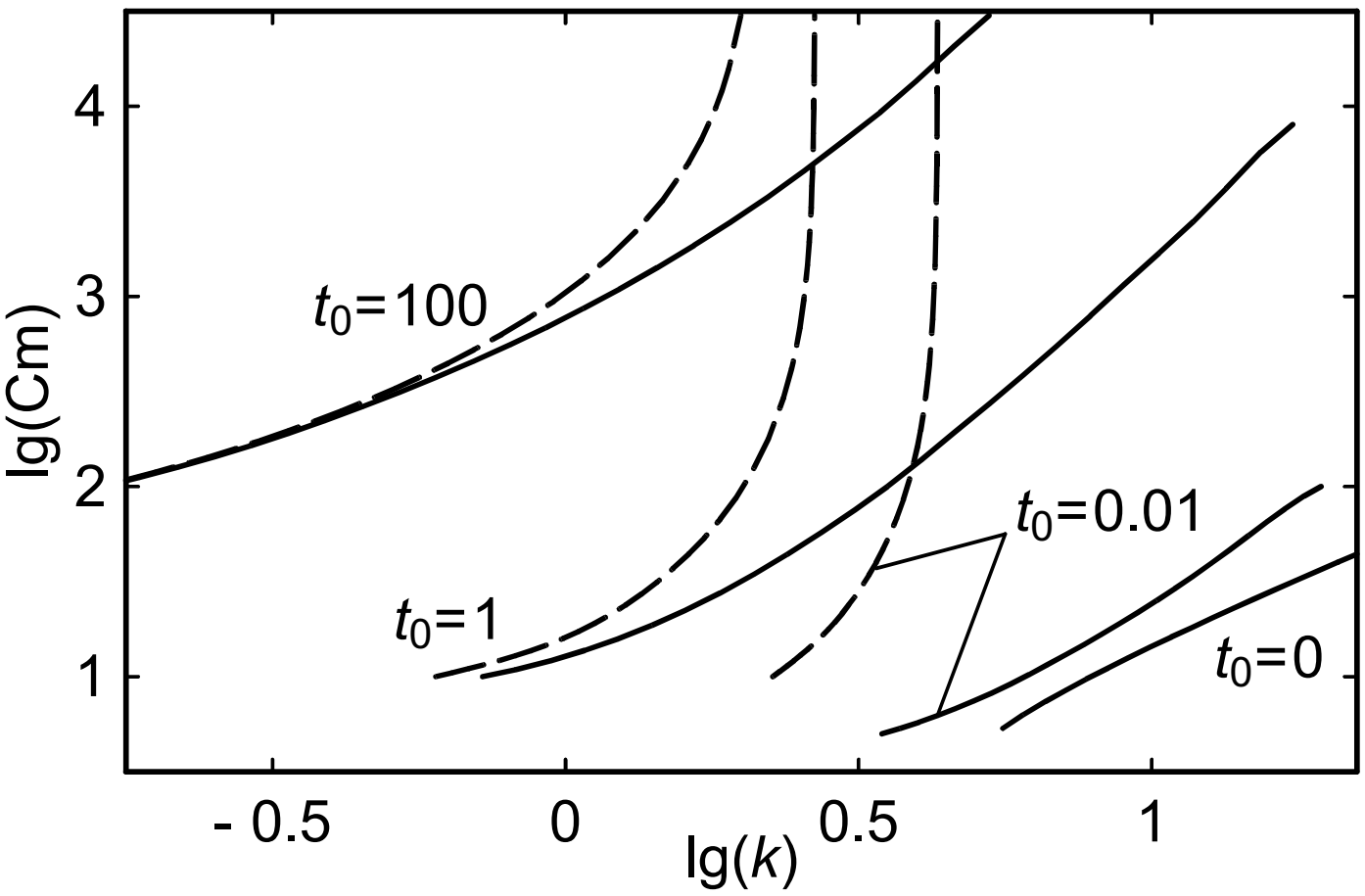

The most unstable wave number of the labyrinthine instability: Darcy (*solid lines*) vs Brinkman (*dashed lines*).

Evolution of the neutral curves: the labyrinthine instability

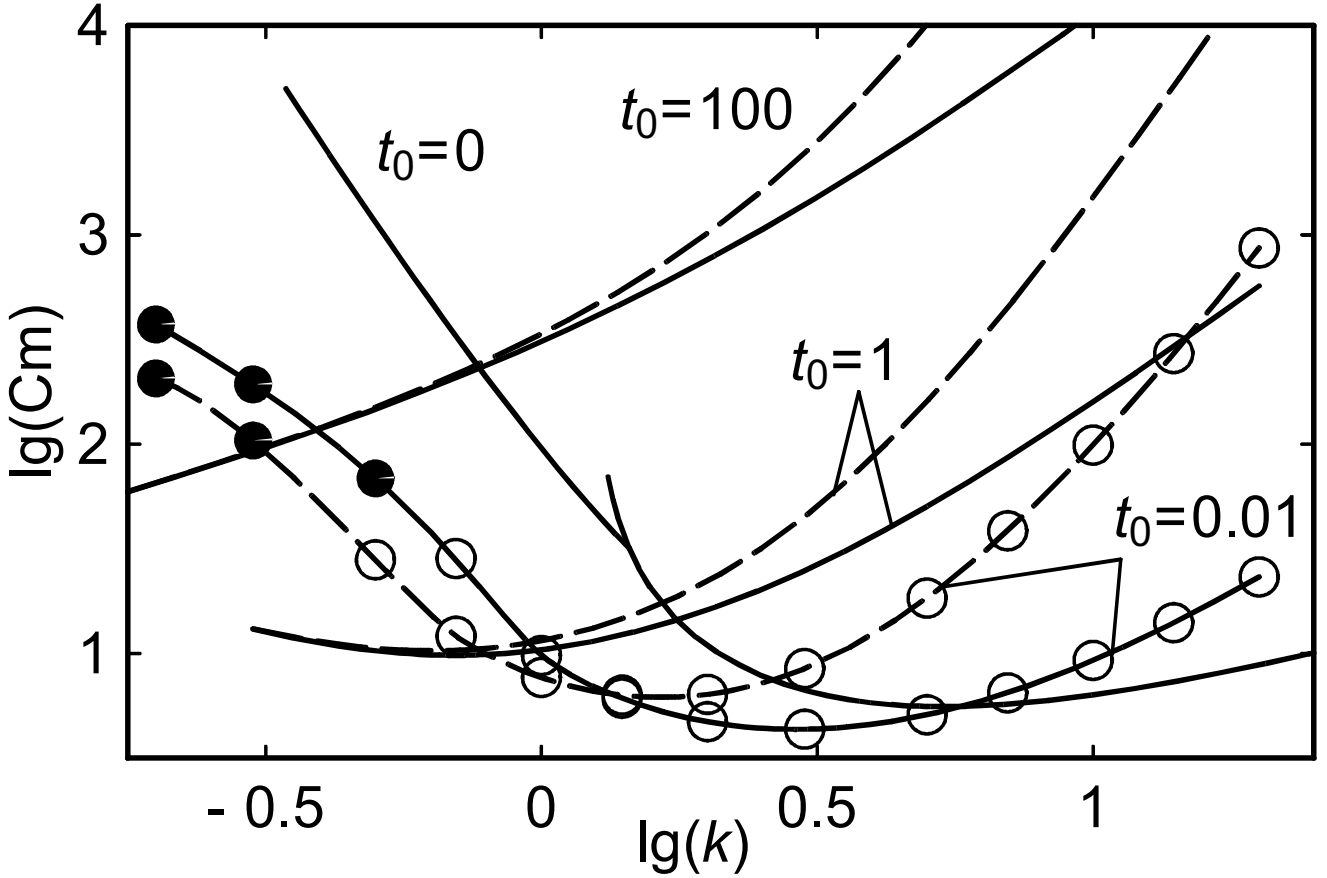

Evolution of the neutral curves for the originally step-like concentration distribution as the basic gradients diffuse out (i.e. as t_0 increases) for the Darcy (*solid lines*) and Brinkman (*dashed lines*) flows. Filled dots denote numerically obtained neutral oscillations, hollow ones – monotonous modes.

Evolution of the neutral curves: the peak instability

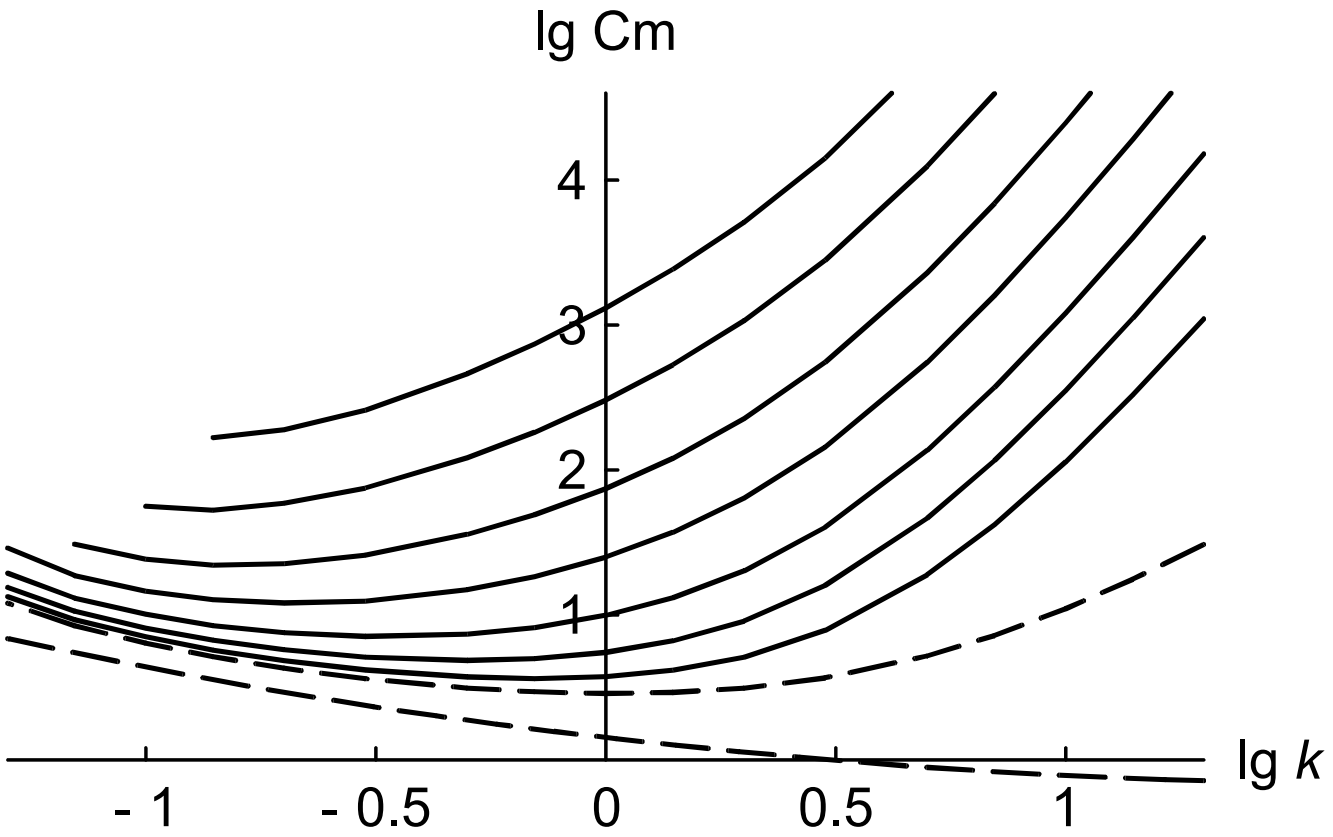

Evolution of the neutral curves for the originally step-like concentration distribution as the basic gradients diffuse out (t_0 increases upwards) for the Brinkman (*solid lines*) and Darcy (*dashed lines*) flows.

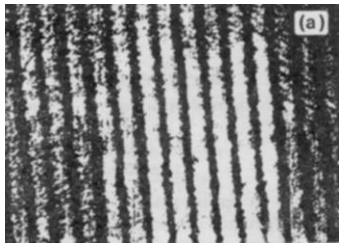

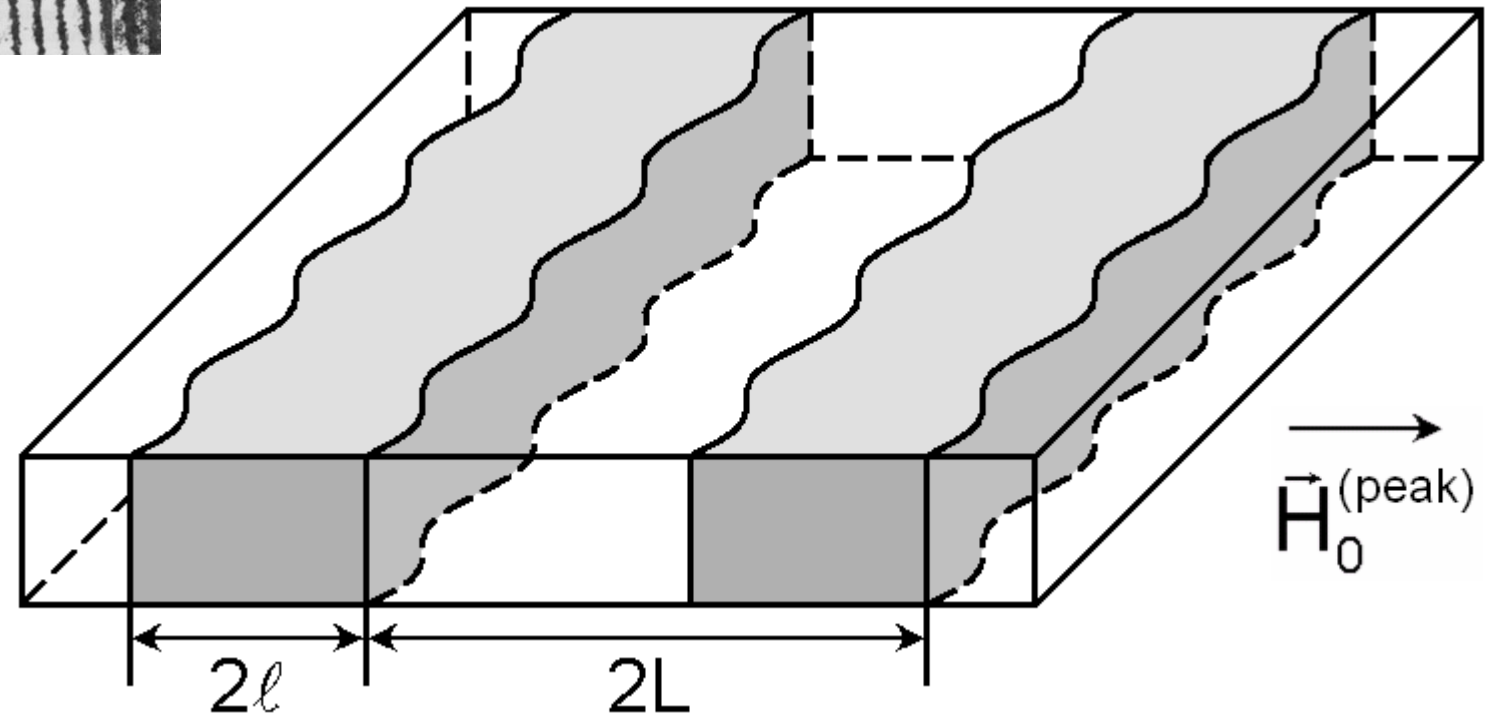

Analytically: an array of sharp parallel stripes

Numerically: a Gaussian concentration distribution $c_2 = \exp\left(-0.25x^2 / t_0\right)$

The neutral curves for the sharp stripes (the Darcy flow)

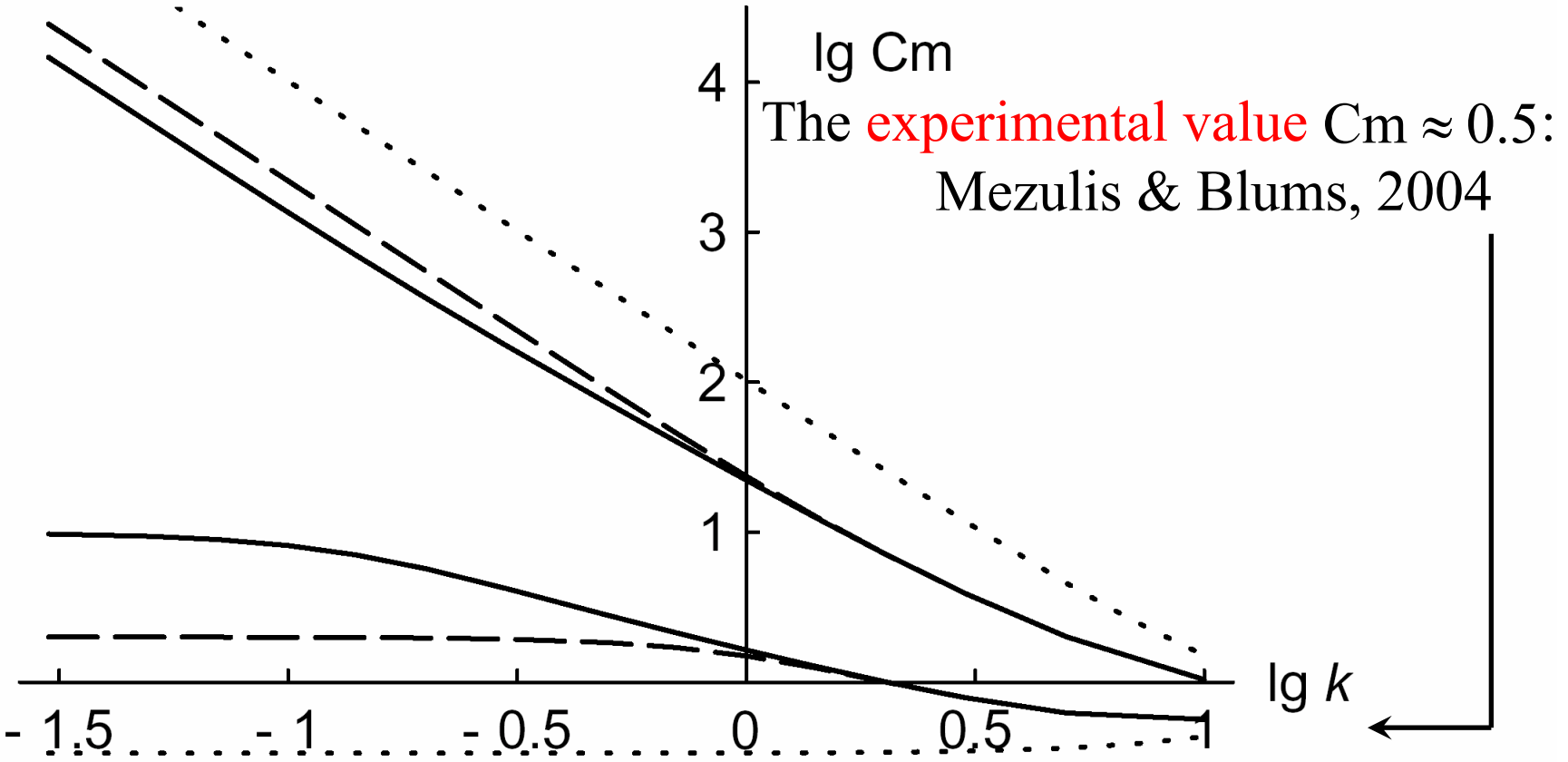

Figure 2.17: The neutral curves for the instability of the periodic array of narrow ($l = 0.1$) sharp stripes in the Darcy flow. *Dotted lines*: $L = 0.2$; *dashed lines*: $L = 2$; *solid lines*: $L = 10$.

Conclusions to Part II.

- The linear stability of an inhomogeneous ferrofluid against convection is analysed – analytically for sharp interfaces and numerically for diffused ones. Inhomogeneous ferrofluid is shown to undergo instability due to the self-magnetic field. Oscillations are found and explained.
- Viscosity and diffusion are equally responsible for the threshold of convection. The Darcy law is usable at the onset of instability. But at strong forcing, the length scale is determined by viscosity alone. This is due to the Brinkman equation which is the simplest one to describe the experimentally observed saturation of the length scale.
- Microconvection in the FRS setup is predicted. The threshold of this instability is in quite good agreement with recent experiments.

Part III.

Immiscible interfaces: The nonlinear simulations of the Saffman–Taylor instability by the boundary-integral method.

Instabilities with immiscible ferrofluids

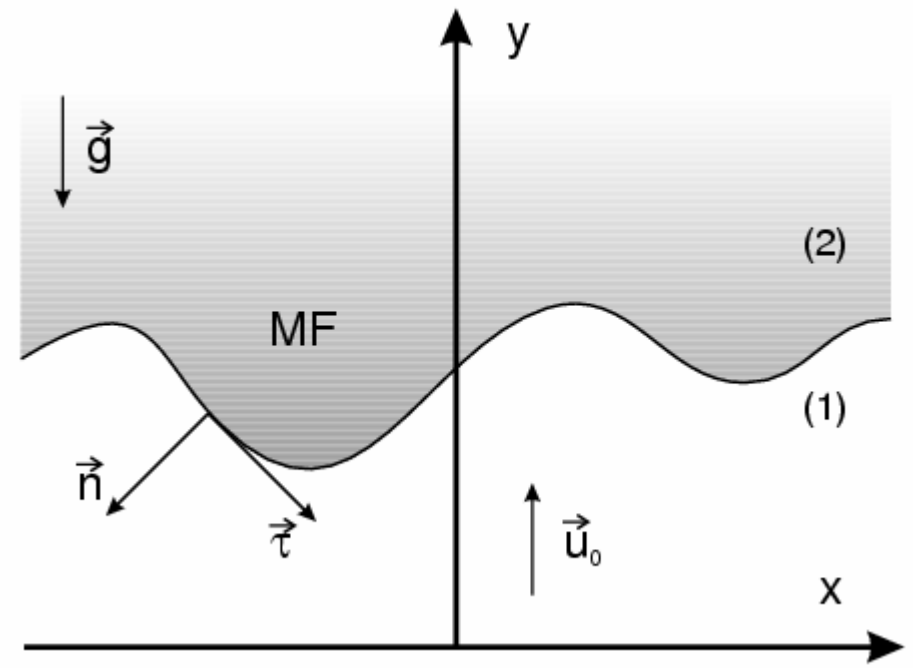

$$\mathrm{Bg} = h^2 g(\rho_2 - \rho_1)/\sigma \qquad \mathrm{Bg} \Leftrightarrow \mathrm{Ca}$$

$$\mathrm{Bm} = 2(M_2 - M_1)^2 h/\sigma$$

$$\mathrm{At} = (\eta_2 - \eta_1)/(\eta_2 + \eta_1) \qquad T$$

The boundary-integral method

$u_x = \partial\psi/\partial y \quad u_y = -\partial\psi/\partial x$ Darcy:

the stream function satisfies $\Delta\psi = 0$. Then $\psi(\vec{r}) = \dfrac{1}{2\pi}\int \gamma(s')\ln|\vec{\rho}(s') - \vec{r}|\,\mathrm{d}s'$

The Cauchy integral $u_x - iu_y = \dfrac{1}{2iT}\int\limits_{\text{period}} \gamma(z')\cot\dfrac{\pi(z'-z)}{T}\,\mathrm{d}z'$

The dynamic boundary condition $[p] = \sigma/R$ becomes

$$\gamma(s) + \mathrm{At}\int\limits_{\text{period}} \gamma(s')N(s,s')\,\mathrm{d}s' = -2\frac{\partial}{\partial\tau}\left(\frac{1}{R} + \mathrm{Bg}\,y + \mathrm{Bm}\,I_{\text{mag}}\right)$$

Cebers, Magnetohydrodynamics 33(2), 99 (1997).

The numerical algorithm

- The discretized interface is interpolated by periodic cubic splines

- Numerical error of the algorithm: $O((\Delta s)^4, (\Delta t)^2)$

This consistency order is indeed observed with the magnetic force.

- Numerical stability is maintained without any filtering.

- Explicit time-stepping: a constraint $(\Delta t)_{\max} \sim (\Delta s)^3_{\min}$

- Validation: linear growth rates, widths of the Saffman–Taylor fingers, existing results …

Baker & Nachbin, SIAM J. Sci. Comput. 19, 1737 (1998);

Hou, Lowengrub, and Shelley, J. Comput. Phys. 114, 312 (1997).

Fingers in the labyrinthine field

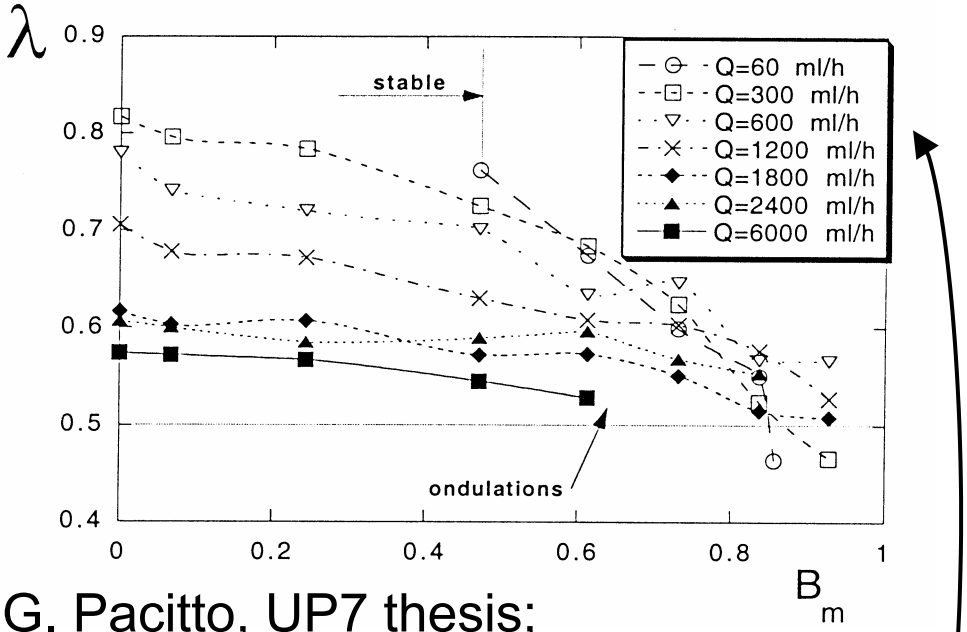

G. Pacitto, UP7 thesis;
Pacitto, Flament, and Bacri,
Phys. Fluids 13, 3196 (2001).

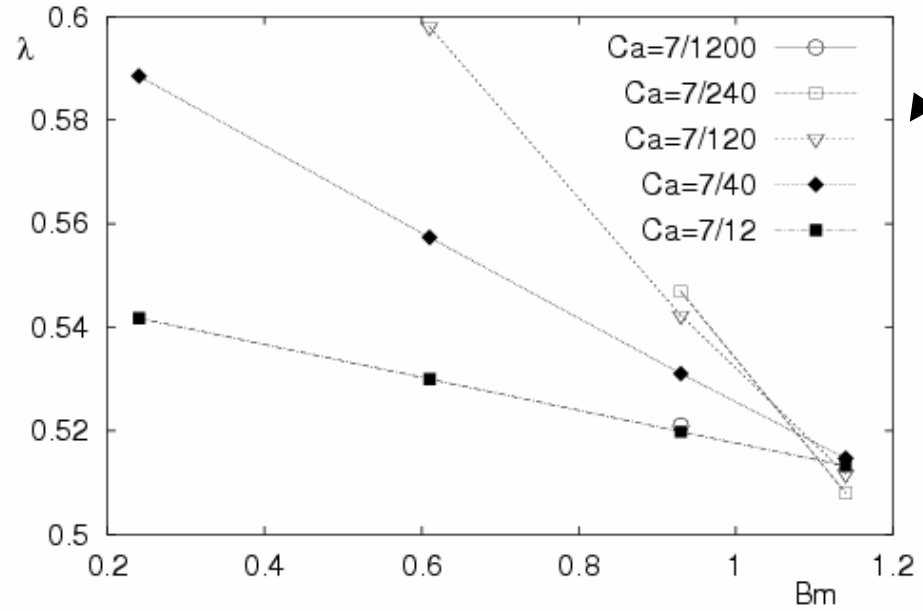

symbols are correspondent

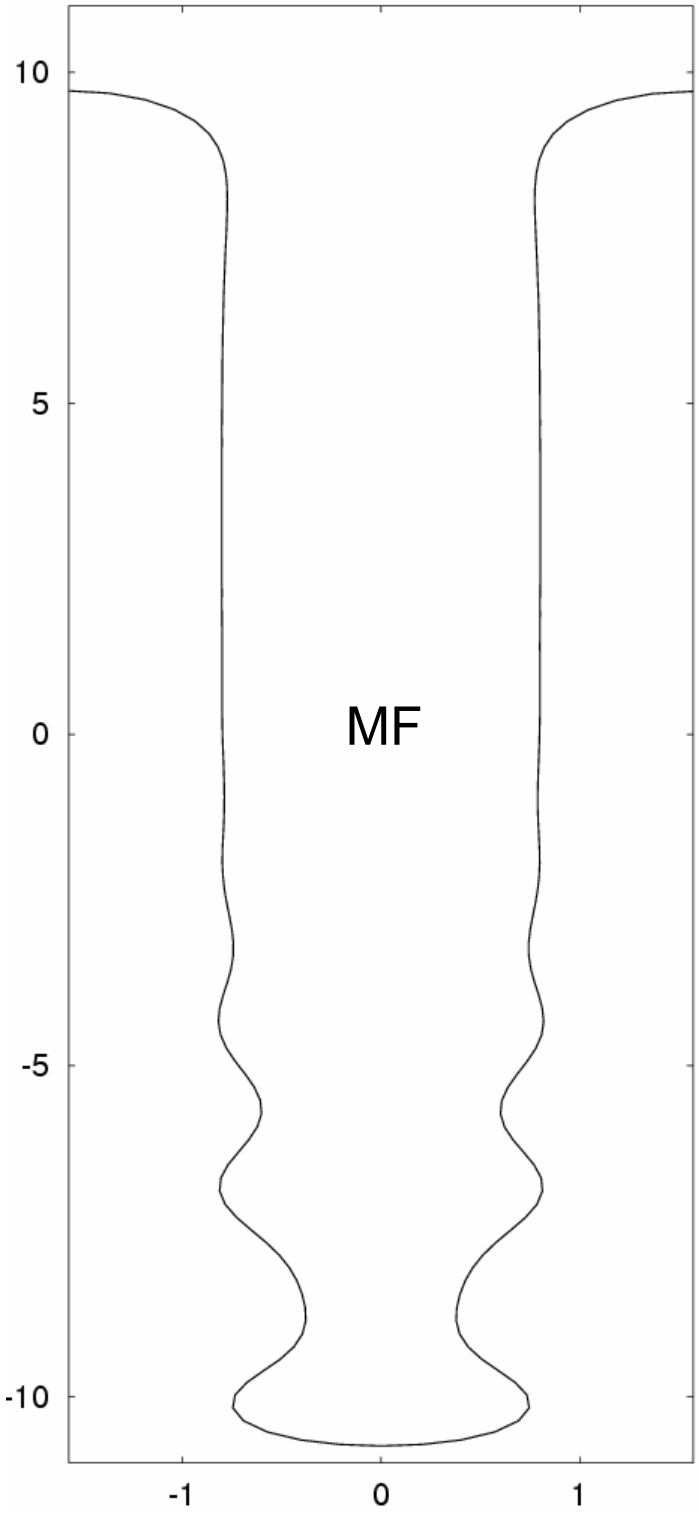

Fingers in the labyrinthine field

Pacitto, Flament, and Bacri, Phys. Fluids 13, 3196 (2001).

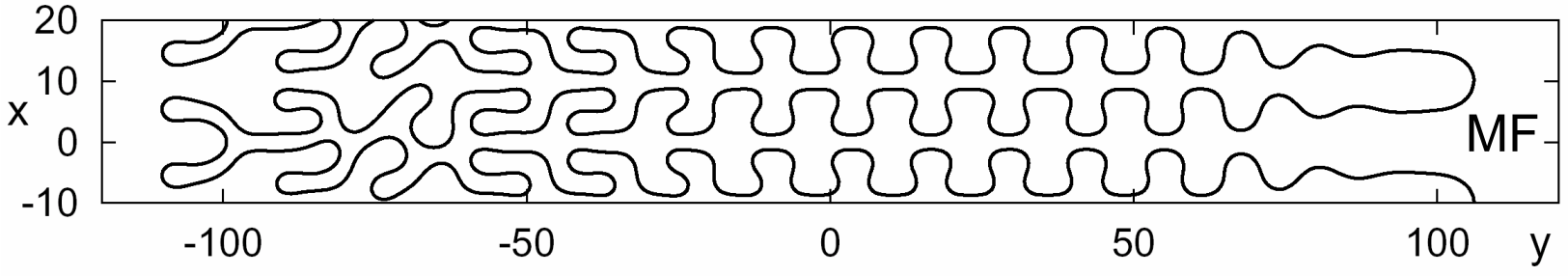

Dendritic patterns

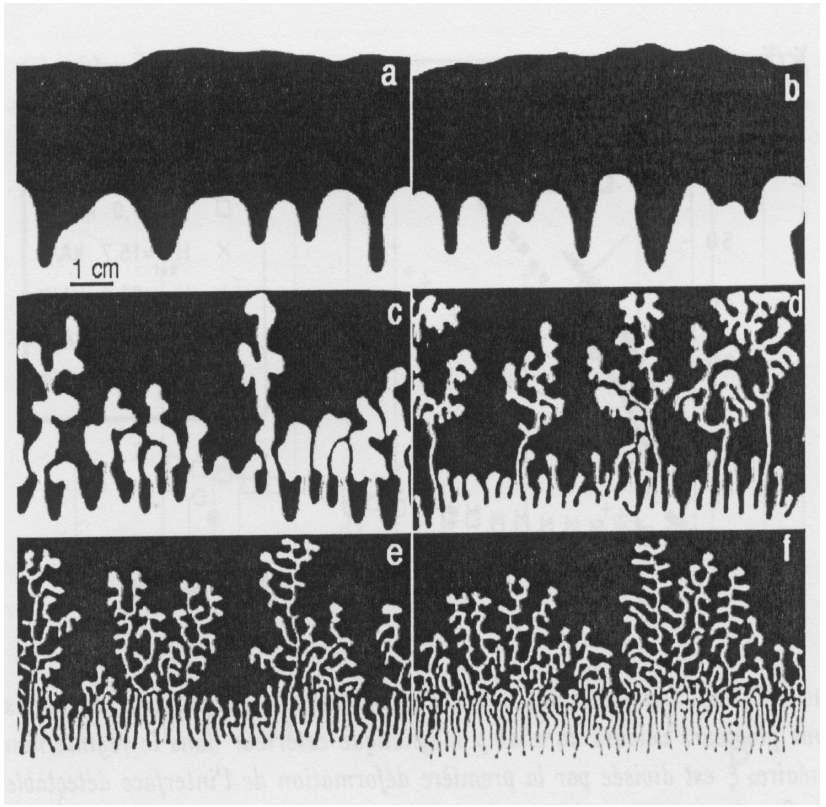

$\vec{H}_0$

$\vec{g}$

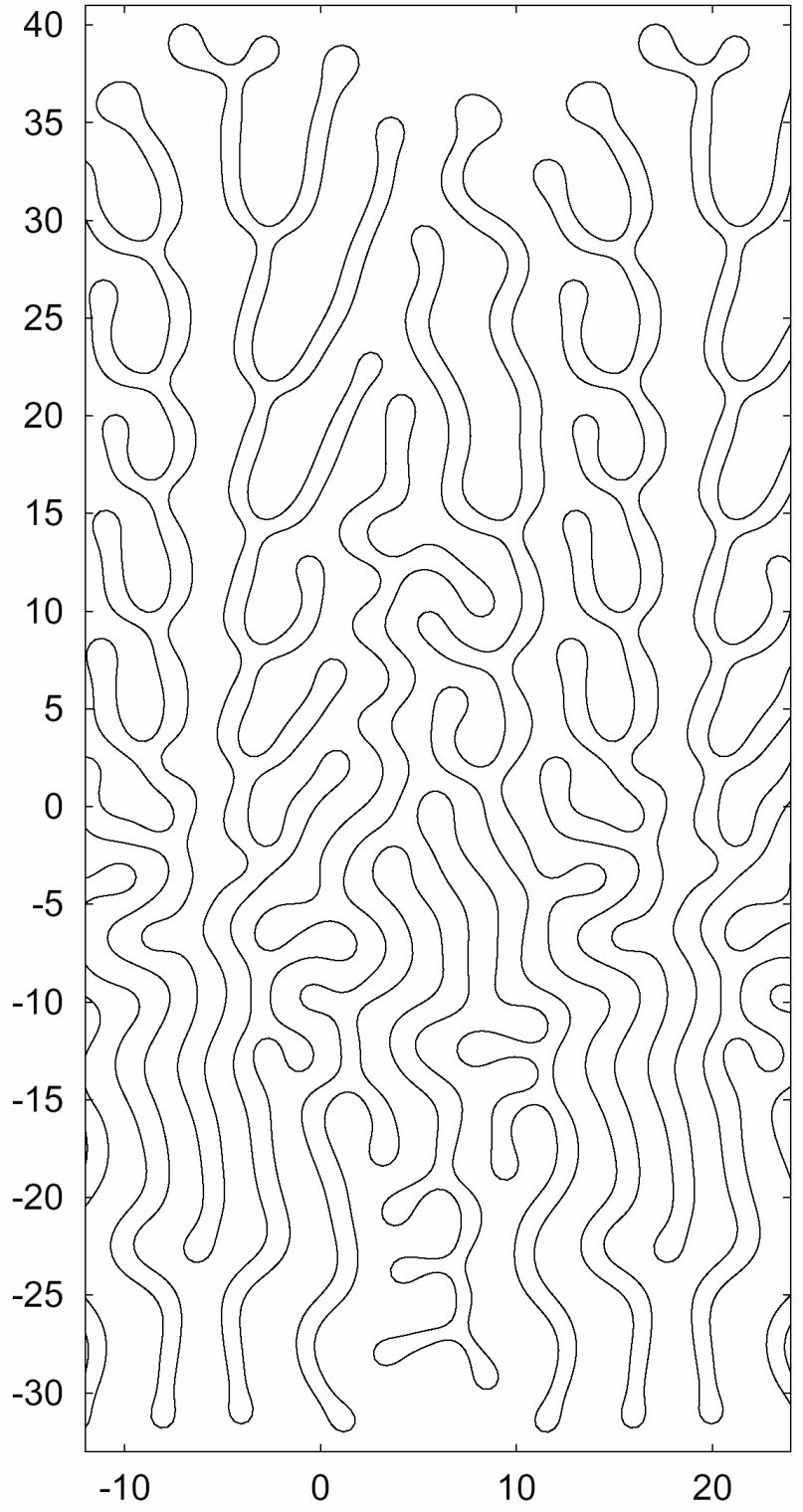

G. Pacitto, UP7 thesis;
Pacitto et al., PRE 62, 7941 (2000)

Chevron / hairpin pattern

$\vec{H}_0$

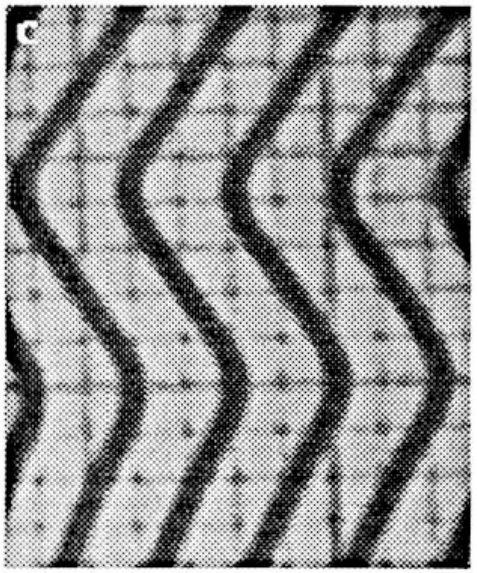

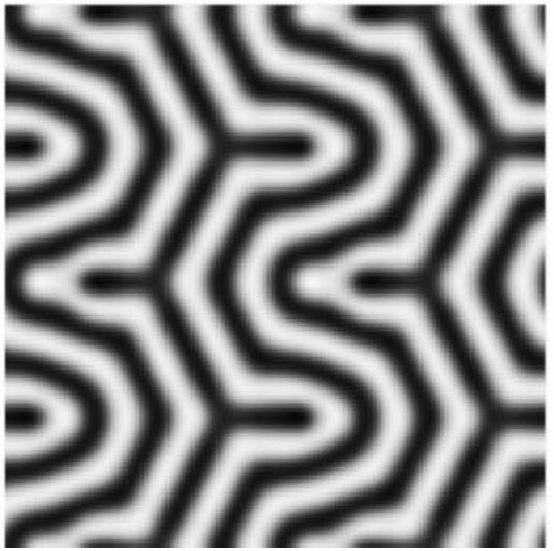

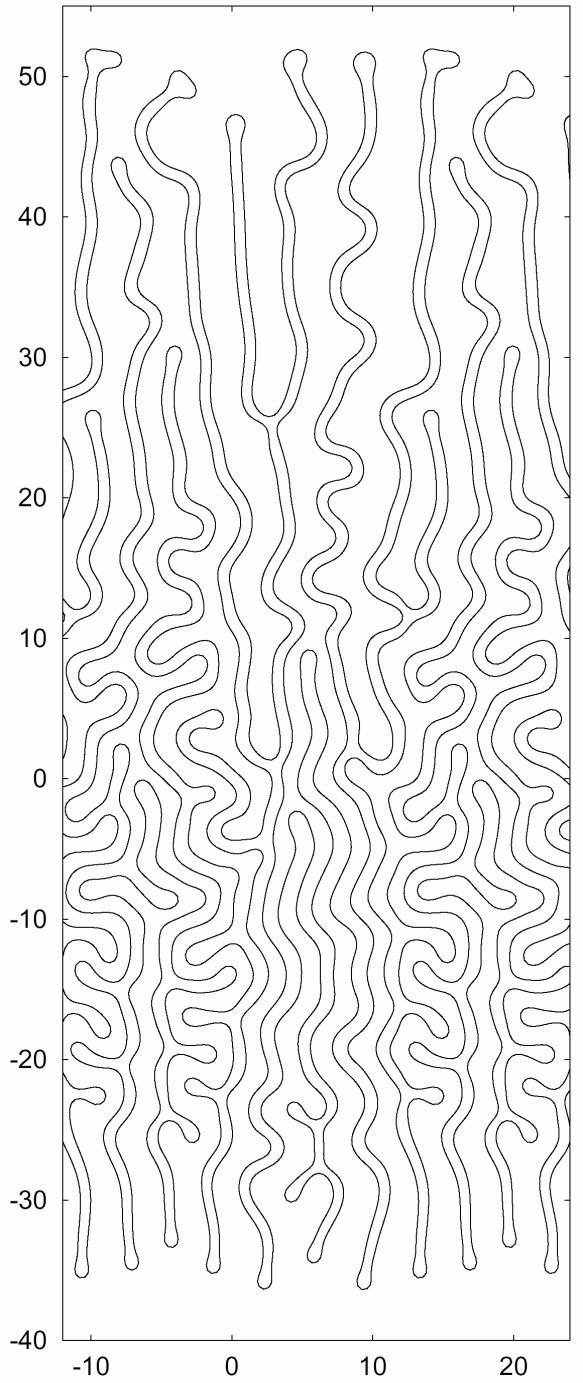

Flament et al.,
Europhys. Lett. 34 (3), 225 (1996).

Cebers,

PRE 61, 700 (2000).

The patterns adapt itself
to the change in the favourable length scale

Fingers in the peak field

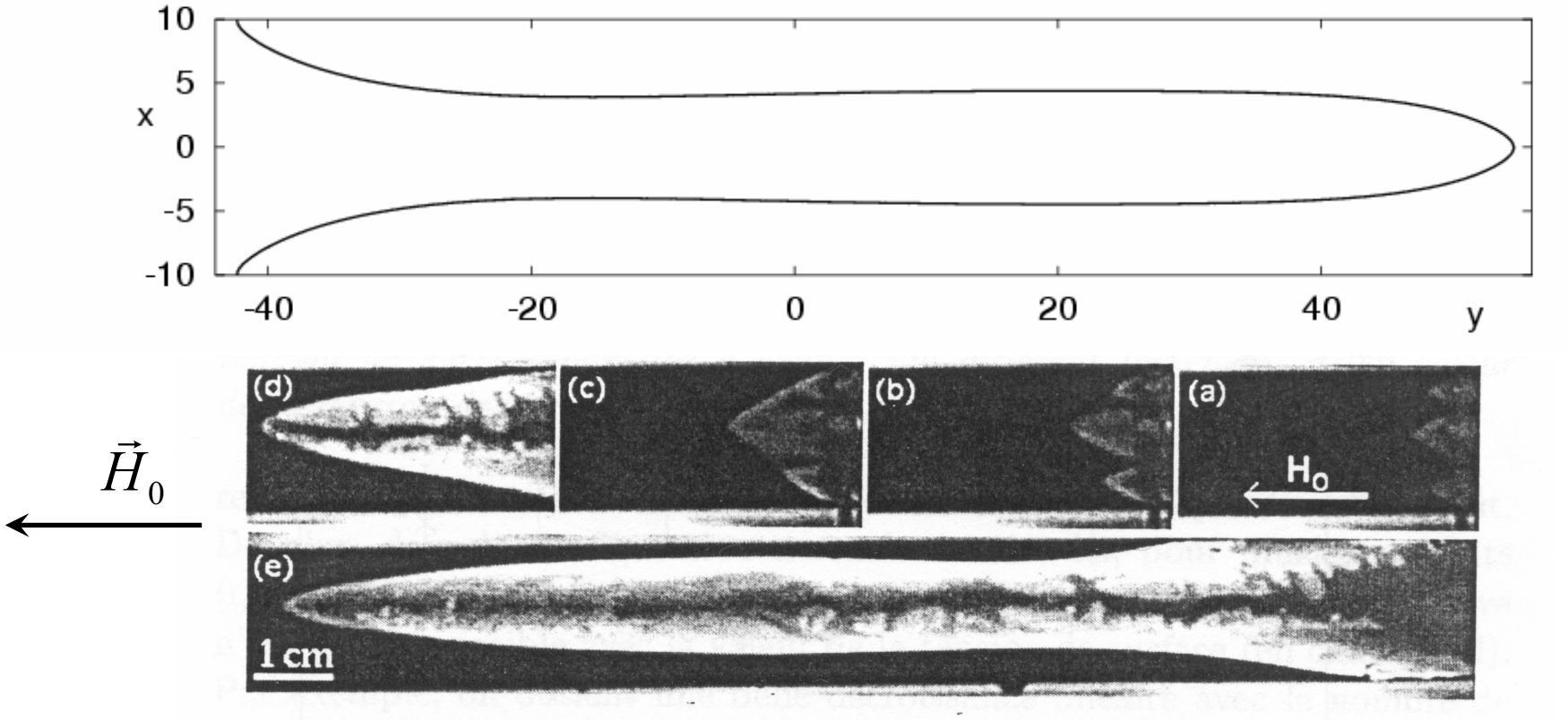

FIG. 2.34 – *Digitation magnético-visqueuse dans la configuration normale pour* $B_m = 0{,}84$ *et* $Q = 100\,ml/h$.

G. Pacitto, UP7 thesis;
Pacitto, Flament, and Bacri, Phys. Fluids 13, 3196 (2001).

Conclusions to Part III.

- The accuracy of the boundary-integral method is improved without impairing the numerical stability.
- We modelled the Saffman–Taylor instability in the presence of long-range dipolar forces. We reproduced some experimentally observed peculiarities and mechanisms of pattern formation: dendritic structures, tip- and vertex-splitting, finger shielding, side-branching, undulations, symmetry breaking...
- We obtained qualitative agreement with experiments for the dependence of the relative finger width on Bm and Ca.

General conclusions

1) The self-magnetic field can cause convective instability.

2) Viscosity and diffusion are equally responsible for the threshold of instability, but at strong forcing, the length scale is determined by viscosity alone and is of the order of the cell thickness.

3) The convection in the FRS setup is predicted in good agreement with recent experiments.

4) High-precision simulations allowed to model the pattern formation due to long-range forces and reproduce experimental observations.

Perspectives

- Non-linear simulations of the miscible problem with the Brinkman equation and possibly with the Korteweg stresses.
- To investigate the possibilities offered by the magnetic microconvection for real microfluidic devices.
- To extend the immiscible simulations: a single ST finger, time-dependent Bm, etc.
- More experiments…